Three-dimensional structure of magnetic skyrmions

R. Brearton ●,[1,2,*] D. M. Burn,[2] A. A. Haghighirad ●,[1,3] G. van der Laan ●,[2,†] and T. Hesjedal ●[1,‡]

[1]*Department of Physics, Clarendon Laboratory, University of Oxford, Oxford OX1 3PU, United Kingdom*
[2]*Diamond Light Source, Harwell Science and Innovation Campus, Fermi Ave, Didcot OX11 0DE, United Kingdom*
[3]*Institute for Quantum Materials and Technologies, Karlsruhe Institute of Technology, 76021 Karlsruhe, Germany*

Magnetic skyrmions (skyrmions hereafter) are magnetization configurations, whose topological robustness and nanoscale size have led to speculation that they could find use as a next-generation information carrier. Skyrmions have been observed in magnetic multilayer materials that are thin compared to the radius of a skyrmion, and chiral cubic single crystals that can be far larger than any characteristic skyrmion scale. In these single crystals, one would expect that skyrmions could exhibit interesting three-dimensional (3D) characteristics. Here, the symmetry of the micromagnetic free energy is investigated. This symmetry permits a complex 3D modulation of a skyrmion string, which we show to be a requirement of a skyrmion coexisting with the conical state. We discuss the implications of this modulation with respect to Thiele's equation and interskyrmion interactions. Further to this internal modulation, we study theoretically and show experimentally that the strings themselves must contort towards the surfaces of their confining crystals.

I. INTRODUCTION

In two dimensions, skyrmions appear as localized whirls of magnetic moments. In three dimensions, the structure of skyrmions is thought to remain roughly constant, and the whirl propagates through the third dimension with a string-like structure [1]. The inverse stereographic projection of the magnetization field hosting a skyrmion is a sphere in which the magnetic moments are mapped onto its surface. This maps the surface precisely once if the winding number is 1. Consequently, calculating its winding number using [2,3]

$$N[\mathbf{m}] = \iint_S \mathbf{m} \cdot (\partial_x \mathbf{m} \times \partial_y \mathbf{m}) dx\, dy, \quad (1)$$

where $\partial_x = \partial/\partial x$, along any surface S not containing the skyrmion string's propagation vector, gives $N = 1$. Consider a deformation of the skyrmion's magnetization $\mathbf{m}$ whose consequence is that the winding number $N[\mathbf{m}]$ decreases below 1. The surface mapped out by the inverse stereographic projection of $\mathbf{m}$ will no longer be the surface of a sphere, but a sphere with a hole in it. As the stereographic projection is a conformal map, this discontinuity in the sphere must manifest itself in $\mathbf{m}$ as a discontinuity in the gradient of the magnetization. For any finite exchange interaction, this deformation would result in a divergent increase in energy. In real materials, this

leads to a substantial energy barrier that prevents skyrmions from being easily deformed into topologically trivial states, such as the uniformly magnetized or conical phases, and so skyrmions are often hailed as being "topologically protected" (an excellent analysis of the topological protection of skyrmions can be found in Ref. [4]).

As well as this topological stability, skyrmions exhibit other fascinating topological behaviors. Consider a skyrmion in an itinerant helimagnet. In the strong Hund's coupling limit, one can think of conduction electrons perfectly exchange coupling to the magnetization. The most simple mathematical construction of the magnetization of a skyrmion is [2,5,6]

$$\mathbf{m} = [C \sin f(r),\ S \sin f(r),\ \cos f(r)], \quad (2)$$

where $C = \cos(N\theta + \gamma)$, $S = \sin(N\theta + \gamma)$, γ is the skyrmion's helicity angle, $f(r)$ is the angle between the magnetization and the z axis, and θ and r are the azimuthal and radial coordinates, respectively. Then, the wave function of conduction electrons becomes $|\chi\rangle = [\cos(f/2), e^{i(N\theta + \gamma)} \sin(f/2)]^\mathsf{T}$ [2,7]. The amplitude for an electron to hop a distance $A\mathbf{e}_k$ from a coordinate $\mathbf{x}$ is then $t(A\mathbf{e}_k) = t \langle \chi(\mathbf{x}) | \chi(\mathbf{x} + A\mathbf{e}_k) \rangle$, where t is the hopping magnitude, A the lattice parameter, and $\mathbf{e}_k$ the unit vector along the kth spatial dimension. This can be written $t(\mathbf{x}, A\mathbf{e}_k) = t e^{i a_k(r) q_e/\hbar c}$, which is nothing but the Peierls factor for hopping in the presence of an applied magnetic field, where q_e is the charge of an electron, c is the speed of light, and $\hbar$ is the reduced Planck constant—the skyrmion appears to source a vector potential of the form $a_k(r) = \frac{\hbar c}{2 q_e}[1 - \cos f(r)]\partial_k N\theta$. Differentiating reveals the remarkable fact that skyrmions give rise to an effective electric and magnetic field, whose ith components are $B_{\mathrm{Sk},i} = \frac{\hbar c}{2 q_e}\epsilon_{ijk}\mathbf{m} \cdot (\partial_j \mathbf{m} \times \partial_k \mathbf{m})$ and $E_{\mathrm{Sk},i} = \frac{\hbar}{2 q_e}\mathbf{m} \cdot (\partial_i \mathbf{m} \times \frac{d\mathbf{m}}{dt})$, respectively, where ϵ_{ijk} is

---

*richard.brearton@physics.ox.ac.uk
†gerrit.vanderlaan@diamond.ac.uk
‡thorsten.hesjedal@physics.ox.ac.uk

the Levi-Civita tensor of rank 3. So, when a skyrmion moves through a medium with conductivity σ, it exerts a spin-transfer torque with a current of magnitude $\mathbf{j} = \sigma \mathbf{E}_{Sk}$ on its surrounding magnetization.

The approach shown above is very common for the investigation of the properties of skyrmions: begin with the magnetization *Ansatz* in Eq. (2) and study its properties in various contexts. Unfortunately, this *Ansatz* has very little physical justification, and is typically introduced using phrases such as "using the symmetry of the skyrmion" without discussion or explanation [2,5,6]. Here we investigate the rotational and translational symmetry of the micromagnetic free energy, deriving constraint equations that, when satisfied by a magnetization field $\mathbf{m}$, show that $\mathbf{m}$ is a symmetry of the free energy.

In general, the three-dimensional structure of skyrmions has the freedom to take a much richer form than shown in Eq. (2). To begin to understand the nature of the complicated three-dimensional states available to skyrmions, the effect of embedding a state inside a topologically distinct phase is investigated. This is applied to the case of a skyrmion being immersed in the conical phase, which is a situation that has been studied previously. In 2016, it was first predicted that skyrmions should acquire an attractive interparticle interaction when coexisting with the cone phase [8]. Such attractive skyrmion clusters were later observed in a Lorentz transmission electron microscopy experiment [9], and a significant amount of research has been carried out on modulated topological structures since, both in magnetic and in liquid-crystal systems [10–17].

Here it is shown analytically that, if a topological state is embedded within a periodic magnetization texture, the topological state must become modulated with the same periodicity as the surrounding phase. This implies that skyrmions embedded in the cone phase should become conically modulated, which provides an important link between a phase coexistence that can be measured experimentally, and the wealth of research carried out on the properties of conically modulated skyrmions. This modulation is studied using computational micromagnetics, agreeing with previous literature. The interactions between conically modulated skyrmions are briefly discussed, and it is shown that one cannot model their dynamics using Thiele's approximate equation of motion.

Finally, the contortion of skyrmion strings near a surface is investigated. Using resonant elastic x-ray scattering (REXS), we show that skyrmions become pinned to their confining surfaces. This is reproduced using computational micromagnetics, where it is found that this is driven by the low energy density of so-called surface twist states, which arise as kink solutions to the sine-Gordon equation.

II. THE SYMMETRY OF THE FREE ENERGY

The free energy for the magnetization field in a ferromagnet without an inversion center takes the form [5,18,19]

$$E = \int_V \mathcal{E}(\mathbf{m}) d^3 x$$

$$= \int_V [\mathcal{E}_J(\mathbf{m}) + \mathcal{E}_D(\mathbf{m}) + \mathcal{E}_B(\mathbf{m})] d^3 x, \quad (3)$$

where $\mathcal{E}_J = J(\nabla \mathbf{m})^2$ is the exchange energy density, $\mathcal{E}_D = D\mathbf{m} \cdot (\nabla \times \mathbf{m})$ is the antisymmetric exchange energy density, $\mathcal{E}_B = -\mathbf{m} \cdot \mathbf{B}$ is the Zeeman energy density, and $\mathcal{E}$ is the total micromagnetic energy density. To probe the symmetry of $\mathcal{E}$, it is prudent to investigate the rotations and translations of $\mathbf{m}$ that leave $\mathcal{E}$, or each of $\mathcal{E}_J$, $\mathcal{E}_D$, and $\mathcal{E}_B$, invariant. Here, we first consider the effect of infinitesimal rotations of the magnetization on $\mathcal{E}$, then look at how infinitesimal translations affect $\mathcal{E}$.

The most general form of an infinitesimal rotation to a vector field v can be written as $\mathbf{v}' = \mathbf{v} + \lim_{\Delta \to 0} \Delta \mathbf{a} \times \mathbf{v}$, where primes refer to rotated/translated quantities throughout, and $\mathbf{a}(\mathbf{x})$ is an arbitrary vector field. So, in general, rotations generated by $\mathbf{a}(\mathbf{x})$ affect the Zeeman energy according to the expression

$$\mathcal{E}_B' = \mathcal{E}_B - \lim_{\Delta \to 0} [\Delta \mathbf{a}(\mathbf{x}) \times \mathbf{m}(\mathbf{x})] \cdot \mathbf{B}(\mathbf{x}). \quad (4)$$

The exchange energy density takes the form $\mathcal{E}_J = (\partial_i m_j)(\partial_i m_j)$, when using Einstein's summation convention. Also using the Levi-Civita tensor to write cross products as $[\mathbf{u} \times \mathbf{v}]_i = \epsilon_{ijk} u_j v_k$, the exchange energy density in the rotated frame is

$$\mathcal{E}_J' = (\partial_i m_j')(\partial_i m_j')$$

$$= \mathcal{E}_J + J \lim_{\Delta \to 0} (2\Delta \partial_i m_j \partial_i \epsilon_{jkl} a_k m_l) + O(\Delta^2). \quad (5)$$

The response of the Dzyaloshinskii-Moriya interaction (DMI) energy to the application of a general rotation to $\mathbf{m}$ can be found similarly. Writing

$$\mathcal{E}_D' = D\mathbf{m}' \cdot (\nabla \times \mathbf{m}'), \quad (6)$$

$$= \lim_{\Delta \to 0} [D(m_i + \Delta \epsilon_{ijk} a_j m_k) \times \epsilon_{ilm} \partial_l (m_m + \Delta \epsilon_{mno} a_n m_o)], \quad (7)$$

keeping only terms $O(\Delta)$, and replacing each contraction of Levi-Civita tensors with products of Kronecker deltas, allows Eq. (7) to take the form

$$\mathcal{E}_D' = \mathcal{E}_D + \lim_{\Delta \to 0} D\Delta \{\mathbf{m} \cdot [(\mathbf{m} \cdot \nabla)\mathbf{a}]$$

$$+ (\mathbf{m} \cdot \mathbf{m})(\nabla \cdot \mathbf{a}) + (\mathbf{m} \cdot \mathbf{a})(\nabla \cdot \mathbf{m})$$

$$- \mathbf{a} \cdot [(\mathbf{m} \cdot \nabla)\mathbf{m}]\} + O(\Delta^2). \quad (8)$$

To understand the symmetry of the free energy under translations, consider infinitesimal translations generated by the vector field $\mathbf{b}(\mathbf{x})$. These act on a vector field $\mathbf{v}$ such that $\mathbf{v}' = \mathbf{v} + \lim_{\Delta \to 0} \Delta (\mathbf{b} \cdot \nabla)\mathbf{v}$. The response of the Zeeman energy to translations of the magnetization is readily found to be

$$\mathcal{E}_B' = \mathcal{E}_B - \lim_{\Delta \to 0} [\Delta (\mathbf{b} \cdot \nabla)\mathbf{m}] \cdot \mathbf{B}. \quad (9)$$

The same translations affect the exchange energy density according to

$$\mathcal{E}_J' = \mathcal{E}_J + J \lim_{\Delta \to 0} 2\Delta \partial_i m_j \partial_i b_k \partial_k m_j + O(\Delta^2), \quad (10)$$

and the antisymmetric exchange energy density becomes

$$\mathcal{E}_D' = \mathcal{E}_D + D \lim_{\Delta \to 0} \Delta \{\mathbf{m} \cdot [\nabla \times (\mathbf{b} \cdot \nabla)\mathbf{m}]$$

$$+ [(\mathbf{b} \cdot \nabla)\mathbf{m}] \cdot (\nabla \times \mathbf{m})\} + O(\Delta^2). \quad (11)$$

Having derived the way that energies are affected by translations and rotations of the magnetization, it is interesting to consider what constraints must be placed on **a**, **b**, and **m** such that the energy density is invariant under rotations and translations.

The most general constraint on **m** imposed by rotations and translations can be found by simply combining each of Eqs. (4), (5), (8), (9), (10), and (11), and is given by

$$
\begin{aligned}
0 = {} & -B_i\epsilon_{ijk}a_j m_k - b_i\partial_i m_j B_j \\
& + 2J(\partial_i m_j \epsilon_{jkl} a_k \partial_i m_l + \partial_i m_j \partial_i b_k \partial_k m_j) \\
& + D[m_i m_l \partial_l a_i - m_i m_i \partial_l a_l + m_i a_i \partial_l m_l - a_j m_k \partial_k m_j \\
& + m_i \epsilon_{ijk} \partial_j b_l (\partial_l m_k) + b_l (\partial_l m_i)\epsilon_{ijk}\partial_j m_k].
\end{aligned}
\tag{12}
$$

In principle, it is possible that some magnetization field **m** satisfies Eq. (12) for nontrivial **a** and **b** in such a way that all or some of the terms in Eq. (12) are finite—this would represent the magnetization with the most nontrivial symmetry under rotations and translations. In a real material, the free energy as given by Eq. (3) is an approximation, so that Eq. (12) is simplified compared to the true constraint a magnetization field must satisfy in order to be symmetric under translation and rotation. As such, a detailed investigation of the solutions of Eq. (12) may not be particularly useful. However, some interesting qualitative information can be gleaned from Eq. (12) by understanding what happens when the individual terms in the equation are zero.

Discussion of rotational invariance. First considering rotations of the Zeeman energy density, from Eq. (4), $\mathcal{E}_B = \mathcal{E}_B'$ when $\mathbf{a}(\mathbf{x}) \parallel \mathbf{B}(\mathbf{x})$. This leads to an unsurprising conclusion: if the magnetization is rotated about the direction of the external field, then the energy density remains constant.

For the exchange energy density to remain invariant under rotations of **m**, it is necessary to require that the rotations are generated by a constant vector **a**, i.e., $\mathbf{a} \neq \mathbf{a}(\mathbf{x})$. Then, Eq. (5) becomes

$$
\begin{aligned}
\mathcal{E}_J' &= \mathcal{E}_J + J \lim_{\Delta \to 0}(2\Delta \partial_i m_j \epsilon_{jkl} a_k \partial_i m_l) + O(\Delta^2) \\
&= \mathcal{E}_J + O(\Delta^2),
\end{aligned}
\tag{13}
$$

where the term $O(\Delta)$ in Eq. (13) vanishes by symmetry under exchange of the dummy j and l indices, using $\epsilon_{jkl} = -\epsilon_{lkj}$ [this is precisely analogous to the vector identity $\mathbf{v} \cdot (\mathbf{a} \times \mathbf{v}) = 0$, but replacing the vector **v** with the tensor $\partial_i m_j$]. The behavior of the Dzyaloshinskii-Moriya energy density under rotations is less trivial, but using the frame invariance of the dot product and the curl, then, from Eq. (6) and the definition of $\mathcal{E}_D$, if

$$
\mathbf{m}' \cdot (\nabla \times \mathbf{m}') = \mathbf{m}' \cdot (\nabla' \times \mathbf{m}'),
\tag{14}
$$

then $\mathcal{E}_D = \mathcal{E}_D'$. This occurs to lowest order in Δ when

$$
\mathbf{m} \times [\Delta(\mathbf{a} \times \nabla) \times \mathbf{m}] = 0,
\tag{15}
$$

which is satisfied when $\nabla \times \mathbf{m} \parallel \mathbf{a}$.

Summary of rotational invariance. The Zeeman energy density is invariant under rotations generated by **a** when **a** is parallel to **B**. The exchange energy density is invariant under constant rotations [$\mathbf{a} \neq \mathbf{a}(\mathbf{x})$]. Combining these two constraints, there is only a rotational symmetry if **B** always

points in the same direction; otherwise **a** would have to rotate to follow **B**, in which case **a** would no longer be constant.

From Eq. (15), the DMI term is invariant only when the curl of the magnetization is parallel to **a**. Also taking into account the exchange and Zeeman constraints, the curl of the magnetization has to be parallel to the external magnetic field, which must be uniform. If these conditions are broken, the free energy will have no rotational symmetry.

Discussion of translational invariance. One could be forgiven for expecting that the Zeeman energy density has translational symmetry when the generator of translations **b** $\parallel$ **B**. This turns out to not be the case. Instead, Eq. (9) vanishes in two cases, which can be more easily understood writing $\mathbf{m}' = \mathbf{m} + \mathcal{T}(\Delta\mathbf{b})\mathbf{m}$, where $\mathcal{T}(\Delta\mathbf{b}) = \lim_{\Delta \to 0}(\Delta\mathbf{b} \cdot \nabla)$ is an operator that maps vectors $\mathbf{v}(\mathbf{x})$ to $\mathbf{v}(\mathbf{x} + \Delta\mathbf{b})$. The first case is when $\mathcal{T}(\Delta\mathbf{b})\mathbf{m} \perp \mathbf{B}$; the second is the trivial $\mathcal{T}(\Delta\mathbf{b})\mathbf{m} = 0$.

The translated exchange energy density in Eq. (10) satisfies $\mathcal{E}_J' = \mathcal{E}_J$ when the gradient of the magnetization is normal to the gradient in the change in magnetization due to translation, where the gradient is taken along each axis in turn. This is difficult to understand intuitively from Eq. (10), but written out in terms of the translation operator $\mathcal{T}$, Eq. (10) becomes

$$
\mathcal{E}_J' = \mathcal{E}_J + 2J(\partial_i\mathbf{m}) \cdot [\partial_i \mathcal{T}(\Delta\mathbf{b})\mathbf{m}] + O(\Delta^2).
\tag{16}
$$

This symmetry may sound esoteric, but a nontrivial example can be found in a simple spin helix, defined by

$$
\mathbf{m}_{\text{Helix}} = M_S[\cos(kz + \phi), \sin(kz + \phi), 0],
\tag{17}
$$

in Cartesian coordinates where M_S is the saturation magnetization, ϕ is an arbitrary phase factor, and $\mathbf{k} = k\hat{\mathbf{z}}$ is the wave vector, which has been set parallel to the z axis without loss of generality. Now the derivatives in Eq. (16) are

$$
\partial_i(\Delta\mathbf{b} \cdot \nabla)\mathbf{m} = -k^2 \Delta b_z \delta_{iz}[\cos kz, \sin kz, 0],
\tag{18}
$$

$$
\partial_i\mathbf{m} = k\delta_{iz}[-\sin kz, \cos kz, 0],
\tag{19}
$$

so that clearly $\mathcal{E}_J' = \mathcal{E}_J$ under arbitrary translations.

The symmetry of the antisymmetric exchange under translations shown in Eq. (11) is also somewhat easier to digest when written out in terms of the translation operator $\mathcal{T}$. Then, the condition for translational symmetry is

$$
\mathbf{m} \cdot [\nabla \times \mathcal{T}(\Delta\mathbf{b})\mathbf{m}] = -\mathcal{T}(\Delta\mathbf{b})\mathbf{m} \cdot (\nabla \times \mathbf{m}),
\tag{20}
$$

which can be read as "The dot product between the curl of the change in magnetization due to translation, and the unperturbed magnetization must equal the negative of the dot product between the change in the magnetization due to translation and the curl of the unperturbed magnetization."

Summary of translational invariance. To satisfy the symmetry of the Zeeman energy density, any change in the magnetization due to the translation must be perpendicular to the magnetic field lines. The symmetry demands for translational invariance of the symmetric and antisymmetric exchange energy densities have much less physically intuitive interpretations than those derived for rotational invariance. The equations themselves are, however, still useful for studying the symmetry of magnetization fields; an example of how to check these symmetries by hand has been provided in Eq. (19).

III. SKYRMIONS IN THE CONICAL PHASE

The coexistence of multiple magnetic phases with identical topology is typically a temporary affair. If two magnetic structures $\mathbf{p}(\mathbf{x})$ and $\mathbf{q}(\mathbf{x})$ coexist and have the same topological winding number N as defined in Eq. (1), the magnetic material will inevitably tend towards hosting exclusively the magnetic structure that has the lowest free energy. While there could be some finite energy barrier that separates $\mathbf{p}(\mathbf{x})$ and $\mathbf{q}(\mathbf{x})$, this will eventually be overcome by thermal fluctuations, with the energy barrier setting the expected lifetime of the higher energy state.

States with distinct topological winding numbers, however, can generally coexist. This is because the energy barrier separating two topologically distinct magnetization structures is, in theory, infinite; any path between two topologically distinct magnetization textures would involve an intermediate state with a divergent exchange energy. In reality, this idealized logic is imperfect. Phonons flip magnetic moments, which can provide the "tear" in the magnetization fabric required to change the topology of magnetic states. Nevertheless, as a guiding principle, one should expect states with different topologies to coexist much more readily than states with equivalent topologies.

A trivial but widely studied example would be the coexistence of a two-dimensional magnetic skyrmion with the field polarized state. The skyrmion has a topological winding number $N = 1$, while the field polarized state has $N = 0$. The two-dimensional skyrmion *Ansatz* given in Eq. (2) describes a skyrmion embedded within the field polarized state—using this construction, writing $\mathbf{m} = \mathbf{m}(r, \theta)$, we have that $\lim_{r \to \infty} \mathbf{m}(r, \theta) = \hat{\mathbf{z}}$, which is uniformly magnetized along the field direction.

Much more complicated is the three-dimensional case of a magnetic skyrmion embedded in the conical state. The above study of the symmetry of the magnetization should be sufficient evidence that there is no simple *Ansatz* that we can justify by symmetry that will describe something as complicated as a skyrmion embedded in the cone phase. However, even with a limited mathematical description of the system, it is possible to make progress.

First, we will define an embedded magnetic state as being a state $\mathbf{m}_1$ satisfying

$$\lim_{r \to \infty} \mathbf{m}_1(r, \theta, z) = \mathbf{m}_\infty(r, \theta, z), \quad (21)$$

so that $\mathbf{m}_1$ coexists with $\mathbf{m}_\infty$. For a skyrmion coexisting with the conical phase, we have

$$\lim_{r \to \infty} \mathbf{m}_1(r, \theta, z) = \mathbf{m}_{\text{Con}}(z), \quad (22)$$

$$\mathbf{m}_{\text{Con}}(z) = [\cos(kz) \sin \chi, \ \sin(kz) \sin \chi, \ \cos \chi], \quad (23)$$

where $\mathbf{m}_{\text{Con}}(z)$ represents the cone phase propagating along the z axis.

Now the challenge is to construct a valid $\mathbf{m}_1$ that can satisfy Eq. (22). To do so, it is useful to express vector fields in terms of a basis that includes, as one of its basis vectors, the conical state. Noticing that the vector

$$\mathbf{m}_\perp(z) = [\cos(kz) \sin \chi, \ -\sin(kz) \sin \chi, \ 0] \quad (24)$$

is orthogonal to $\mathbf{m}_{\text{Con}}$ in Eq. (23) throughout all space, a convenient orthonormal basis for vector fields is given by

$$\hat{\mathbf{e}}_1 = \mathbf{m}_{\text{Con}}(z), \quad (25)$$

$$\hat{\mathbf{e}}_2 = \mathbf{m}_\perp(z), \quad (26)$$

$$\hat{\mathbf{e}}_3 = \hat{\mathbf{e}}_1 \times \hat{\mathbf{e}}_2. \quad (27)$$

In this basis, any localized configuration $\mathbf{m}_1$ satisfying Eq. (22) can be written as

$$\mathbf{m}_1 = C_g \cos R(\mathbf{x}) \hat{\mathbf{e}}_2 + S_g \cos R(\mathbf{x}) \hat{\mathbf{e}}_e + \sin R(\mathbf{x}) \hat{\mathbf{e}}_1, \quad (28)$$

where $C_g = \cos g(\mathbf{x})$, $S_g = \sin g(\mathbf{x})$, $g(\mathbf{x})$ is an arbitrary function of $\mathbf{x}$ that controls the internal structure of $\mathbf{m}_1$ and $R(\mathbf{x}) = R(r, \theta, z)$ determines the projection of a state along the conical direction. Applying the limit in Eq. (22) to Eq. (28) yields the requirement

$$\lim_{r \to \infty} R(r, \theta, z) = \pi/2. \quad (29)$$

Derivatives of Eq. (29) give $\lim_{r \to \infty} \partial_\theta R(r, \theta, z) = \lim_{r \to \infty} \partial_z R(r, \theta, z) = 0$, so that the most general form of $R(r, \theta, z)$ is given by

$$R(r, \theta, z) = \rho_{\pi/2}(r) + \rho_0(r) R_{\theta, z}(\theta, z), \quad (30)$$

where $\lim_{r \to \infty} \rho_n(r) = n$.

Now that some constraints have been applied to $R(r, \theta, z)$, it is interesting to consider how to construct a state $\mathbf{m}_1 = \mathbf{m}_{\text{NoCone}}$ that has absolutely no conical modulation (i.e., $\partial_z \mathbf{m}_{\text{NoCone}} = 0$). Choosing $\mathbf{m}_{\text{NoCone}} = [x_0(r, \theta), y_0(r, \theta), z_0(r, \theta)]$ and solving the simultaneous equations

$$a \hat{\mathbf{e}}_1 + b \hat{\mathbf{e}}_2 + c \hat{\mathbf{e}}_3 = x_0 \hat{\mathbf{x}} + y_0 \hat{\mathbf{y}} + z_0 \hat{\mathbf{z}} \quad (31)$$

gives the expression for a (found using the Gaussian elimination method numerically),

$$a = \frac{x_0 \cos kz + y_0 \sin kz + z_0 \cot \chi \cos 2kz}{\sin \chi + \cos \chi \cot \chi \cos 2kz}, \quad (32)$$

so that, if $\mathbf{m}_1$ is to be independent of the z coordinate, the function $R(r, \theta, z)$ must satisfy the equation

$$R(r, \theta, z)_{\text{NoCone}} = \sin^{-1}[a(r, \theta, z)]. \quad (33)$$

If, for some finite interval $r \in [a, b]$, $a, b \in \mathcal{R}_{>0}$, $\rho_{\pi/2}(r) = 0$, and $\rho_0(r) R_{\theta, z}(\theta, z) = R_{\text{NoCone}}$, then it is possible, in this region, for $\mathbf{m}_1$ to be independent of z. However, as $\lim_{r \to \infty} \rho_{\pi/2}(r) = \pi/2$ and $\lim_{r \to \infty} \rho_0 = 0$, if $|b - a| > \epsilon$ for any $\epsilon > 0$, then the ρ_n, and by extension $R(r, \theta, z)$ and $\mathbf{m}_1$, are not analytic. Therefore, if $\mathbf{m}_1$ is an analytic vector field, it cannot be independent of the z coordinate.

The above proof that $\mathbf{m}_1$ cannot be independent of the z coordinate is identical to the proof that the dependence of $\mathbf{m}_1$ on the z coordinate cannot be different than the dependence of the basis vectors on the z coordinate. To show that $\mathbf{m}_1$ must not be independent of the axial coordinate, the functions $x_0(r, \theta)$, $y_0(r, \theta)$, and $z_0(r, \theta)$ were not allowed to vary with z. However, if the functions x_0, y_0, and z_0 were allowed to vary arbitrarily with z, the proof is identical, with the only changes being that $x_0(r, \theta) \to x_0(r, \theta, z)$, $y_0(r, \theta) \to y_0(r, \theta, z)$, and $z_0(r, \theta) \to z_0(r, \theta, z)$. Again it is found that the basis vectors $\hat{\mathbf{e}}_1$, $\hat{\mathbf{e}}_2$, and
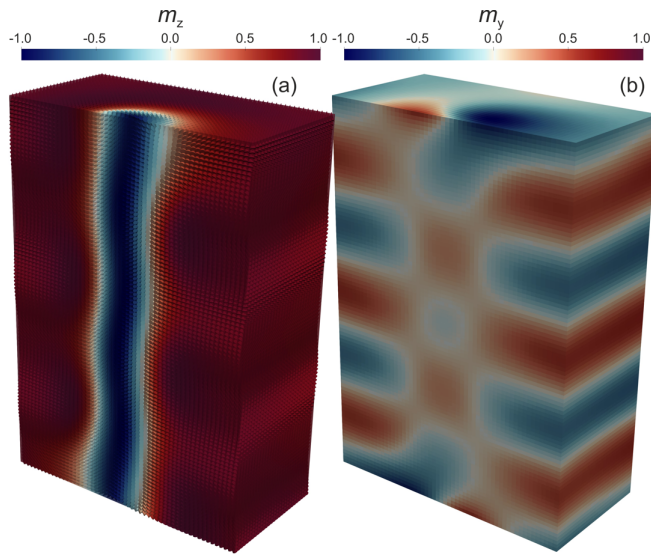
FIG. 1. A slice through a simulation of the conically modulated skyrmion state. (a) The skyrmion string propagates along the z axis, shifting left and right as it progresses, represented by cones which point parallel to the magnetization and are colored by the z component of the magnetization. (b) As in (a), but the surface of the slice is colored by the y component of the magnetization.

$\hat{\mathbf{e}}_3$ are incapable of simultaneously satisfying the localization constraint in Eq. (22) and allowing $\mathbf{m}_1 = x_0\hat{\mathbf{x}} + y_0\hat{\mathbf{y}} + z_0\hat{\mathbf{z}}$ for a finite region of r.

Therefore, if $\mathbf{m}_1$ is an analytic vector field embedded within the conical state, it must be conically modulated.

Internal structure. While the above argument provides strong evidence for the fact that the skyrmion state ought to

be conically modulated in some way when coexisting with the cone phase, it gives very little insight into the internal structure of skyrmions embedded in the cone phase. This is a case that has been studied numerically before [8,9], but a visualization is provided here for reference in Fig. 1. The skyrmion can be seen to oscillate internally with exactly the same periodicity as the surrounding conical state, with a π phase offset.

In addition to having a much richer internal structure, skyrmions embedded within the cone phase exhibit unusual interparticle interactions. Skyrmions that are embedded in a uniformly magnetized state are well understood to have repulsive interactions [5,20]. This is very common for magnetic multilayer systems with interfacial DMI that host skyrmions. Recently, attractive skyrmion clusters have been observed both in numerical calculations and experiment. It has been found numerically that skyrmions become attractive when coexisting with the cone phase, which has been used to explain experimental observations of attractive skyrmions [8,9]. A bound state of two attractive conically modulated skyrmions is also provided here in Fig. 2.

As the bound state in Fig. 2 is localized in the cone phase, the bound state must be conically modulated. This modulation is most easily seen in Fig. 2(c), where the x component of the magnetization oscillates with the same period as the surrounding conical state. A recent scattering study of the coexistence of reflections associated with the skyrmion lattice phase and the conical phase lends further credence to the hypothesis that experimental measurements of attractive skyrmion clusters are due to conically modulated skyrmions [21].

Thiele's equation. Thiele's equation is a simple semiclassical model of the motion of magnetic domains [22]. This has gained popularity recently in the field of skyrmionics
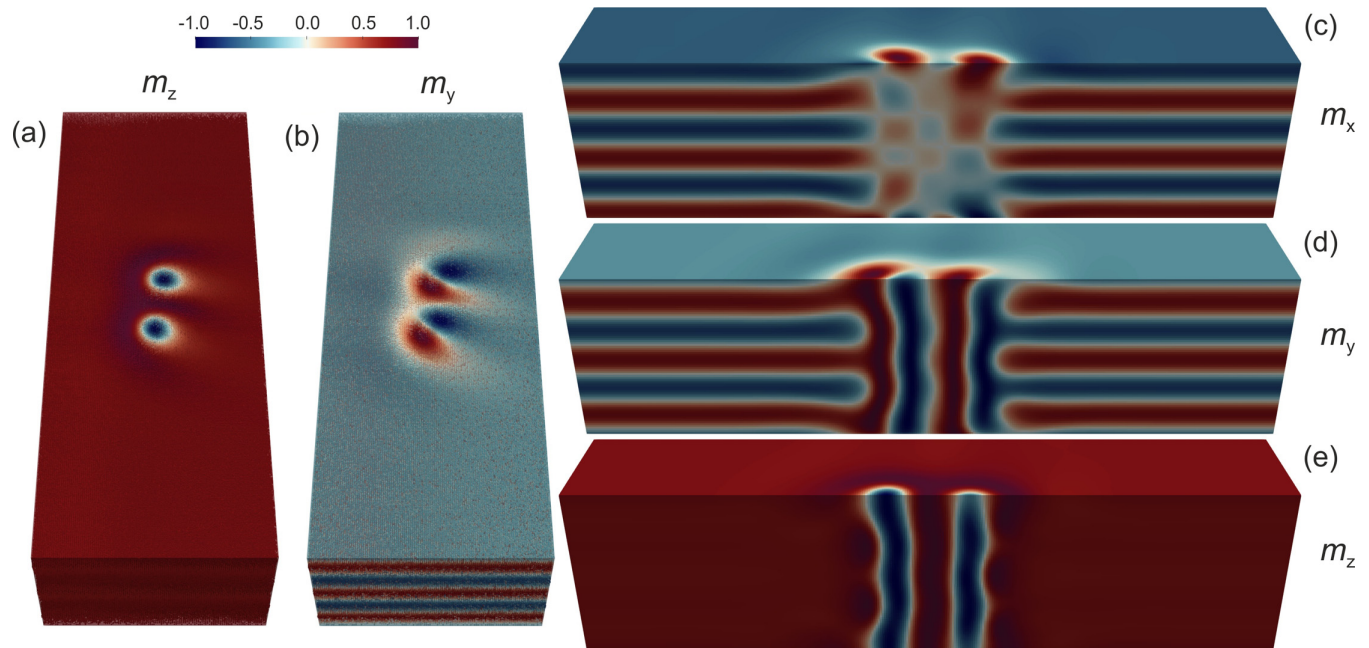

FIG. 2. Conically modulated skyrmions in three dimensions interact attractively and form bound states. (a) An aerial view of the bound state, where the magnetization is represented by cones whose orientation is set by the magnetization, and the color is set by the z component of the magnetization. (b) As in (a), but colored by the y component of the magnetization. (c)–(e) A cross section normal to the y axis through the bound state, where the surface is colored by the x, y, and z components of the magnetization, respectively.

as the interaction potential between two isolated repulsive skyrmions [taking the simple form given in Eq. (2)], which needs to be known to use Thiele's approach, has been well studied [5,20,23]. Integrating Thiele's equation is vastly more computationally efficient than computational micromagnetics, as in conventional computational micromagnetics a skyrmion is constructed from a very large number of finite difference cells, whereas using Thiele's approach only the skyrmion's position needs to be tracked.

A core assumption made to derive Thiele's equation is that the internal structure of a magnetic domain must remain constant. As can be seen from a glance at Fig. 2, this is not the case. The bound conical skyrmion state deforms each of the constituent skyrmions in a different and nontrivial way. Even if an approximate attractive interaction potential could be derived for these modulated skyrmions, Thiele's equation would be invalid as additional energy dissipation would occur as a result of the modification of the individual skyrmion's internal structure.

Summary. In this section, it has been shown that if skyrmions are embedded within the cone phase, skyrmions themselves must become modulated with the same periodicity of the conical state. The approach taken generalizes well to any topologically distinct magnetization configurations. While conically modulated skyrmions have been studied before, the purpose of this section is to provide strong mathematical evidence for their existence whenever skyrmions are surrounded by the cone phase. We anticipate that this will be particularly useful in scattering experiments. It is relatively straightforward to observe the conical state in diffraction experiments by looking for magnetic peaks along the direction of the applied magnetic field. If any scattering peaks associated with a topological magnetic phase are measured simultaneously to the conical reflections, as in Ref. [21], one can say with confidence that the topological phase will be conically modulated, which could significantly affect the physics of the topological object.

It has also been emphasized that, because conically modulated skyrmions form a bound state affecting their internal structure, Thiele's equation cannot be used to model their motion.

IV. THE SURFACE-PINNED SKYRMION STATE

In the previous section, the internal structure of a skyrmion string as it propagates along the z axis have been explored, but it was assumed that a skyrmion string would not deviate spatially from its path along the z axis, where the z axis is defined by the externally applied magnetic field. Here we show that this does in fact occur at the surfaces of materials when the surface normal is not parallel to the magnetic field lines. In this sense, skyrmion strings appear to be pinned to the surfaces of their confining materials.

A. REXS

To study this effect, a REXS experiment at the Cu L_3 resonance was carried out on a sample of Cu_2OSeO_3 using beamline I10 at the Diamond Light Source (Didcot, UK) [24,25]. The sample was aligned so that a (001) face was

out of plane, and the diffractometer was set up such that the scattering vector of the x rays was parallel to (001). Adjacent to this (001) face was the (011) face, from which the x rays were scattered. The magnetic field was applied along the (001) direction throughout. The sample was kept at a temperature of 56.5 K with a measured T_C of 57.5 K, and the magnitude of the magnetic field was 20 mT.

REXS from a face that is not parallel to the scattering q vector has a significant complication: magnetic truncation rods are rotated by the angle between the q vector and the surface normal [26–28]. In the case of scattering from the (011) face with a q vector parallel to the (001), the truncation rods are rotated by 45°. As a result, even the scattering pattern from a skyrmion lattice propagating along the (001) direction will show a significant distortion when measured from a (011) face, as the penetration depth of x rays at resonance is very shallow.

A graphic showing the reciprocal space geometry of scattering from a skyrmion lattice pinned to a face that is not normal to the scattering vector is shown in Fig. 3(a). In this figure, the translucent sphere is the Ewald sphere for the (001) reflection and the brown surface is an approximate representation of the region of reciprocal space sampled by an area detector. This region will be referred to hereafter as the detector's reciprocal surface. A close-up of the detector's reciprocal surface is shown in Figs. 3(b) and 3(c), where Fig. 3(b) assumes that the skyrmions are pinned to the surface normal, and Fig. 3(c) assumes that skyrmions propagate along the (001). In these figures, the magnetic reciprocal lattice is represented by blue spheres, while the magnetic truncation rods are represented by blue cylinders.

What is observed on detector images is the intersection between the detector's reciprocal surface and features in reciprocal space. At the Cu L_3 resonance, the penetration depth for REXS is very small [29] and, correspondingly, the truncation rods are very long. So, typically one measures the intersection between magnetic truncation rods and the detector's reciprocal surface, not the magnetic reciprocal lattice itself. Assuming that skyrmions are pinned to propagate parallel to the surface normal, the intersection between the detector's reciprocal surface and the magnetic truncation rods is shown in Fig. 3(d). The intersection between magnetic truncation rods and the detector's reciprocal surface, assuming that skyrmions are free to propagate along the field direction [which was along the (001) direction], is shown in Fig. 3(e). Crucially, these two scattering patterns look almost identical.

A single image captured on the area detector is shown in Fig. 3(f). Because of the similarities between Figs. 3(d) and 3(e), it is impossible to determine from this data alone which direction the skyrmion lattice is propagating along.

To remove this ambiguity, the same experiment was performed at 5 eV below the Cu L_3 edge. This has two effects. Firstly, penetration depth significantly increases and the magnetic reciprocal space becomes pointlike [28,29]. This means that not all six peaks can be seen simultaneously on a single detector image, as in Fig. 3(f). The second consequence is that scattered intensity is drastically decreased. This was compensated for by increasing the exposure time of the CCD camera. Individual detector frames acquired off
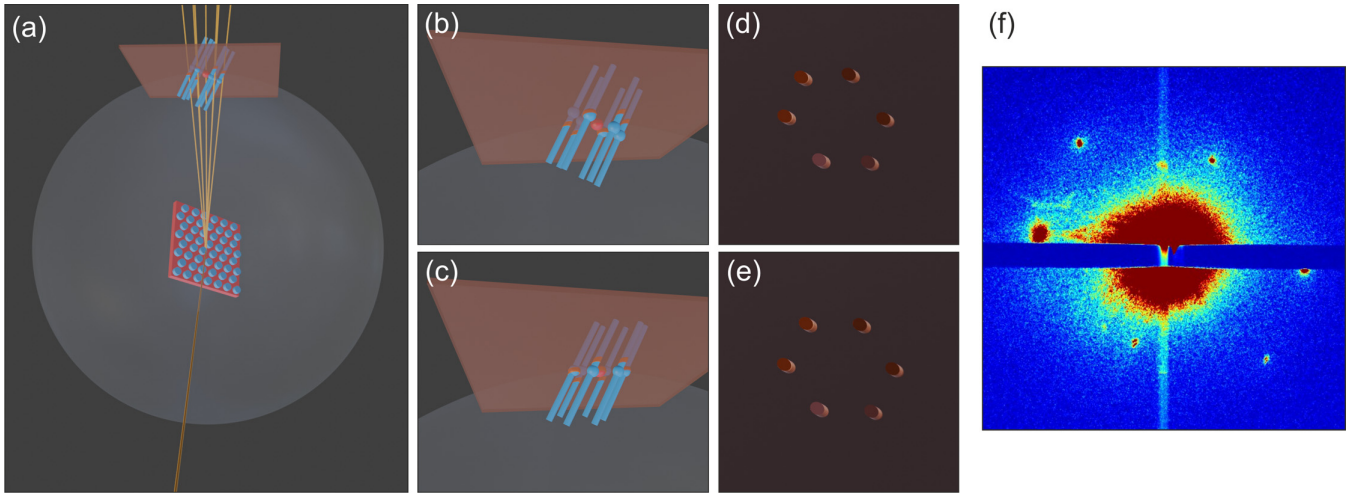
FIG. 3. (a) Geometry of the surface-pinned skyrmion scattering. The sample surface normal is not parallel to the scattering vector, or even in the scattering plane. The skyrmion lattice is taken to be pinned to the surface normal. (b) Close-up of the intersection between the detector's reciprocal surface and the truncation rods from the surface-pinned skyrmion state shown in (a). (c) As in (b), but assuming that skyrmions are *not* pinned to the surface. (d) The intersections between the magnetic truncation rods in (b) and the detector's reciprocal surface. (e) The intersections between the magnetic truncation rods in (c) and the detector's reciprocal surface. (f) A REXS pattern obtained from the (011) face of a crystal of Cu_2OSeO_3 where the field and scattering vectors are both aligned along the (001) direction.

resonance are shown in Figs. 4(a) and 4(b), and the average over these off-resonance frames is shown in Fig. 4(c). The vertical streaks of intensity in Fig. 4 are a trivial consequence of the low scattered intensity in these images; they originate from a line of damaged pixels in the detector and can be ignored. Crucially, the major axis of the ellipse on which the magnetic signal lies is not parallel to the detector vertical, which is possible only if skyrmions are pinned to the surface of their confining material—if the skyrmion strings were parallel to the applied field at the surface, then the major axis of the ellipse of intensity recorded in Fig. 4(c) would be parallel to the vertical of the detector, as in Refs. [24,25].

B. Modeling

To investigate this numerically, a wedge was cut from a cuboid with dimension $420 \times 140 \times 480$ nm^3 and finite difference cells of volume $2.5 \times 2.5 \times 2$ nm^3. Setting the exchange and antisymmetric exchange interactions, as well as the saturation magnetization, to be the values of a generic, well-studied noncentrosymmetric crystal (FeGe), the external field was set to 286 mT. For simplicity [and consistency with the free energy in Eq. (3)] demagnetizing effects were neglected, which is why the external field value is so large.

The system was initialized with nine equally spaced skyrmionlike strings propagating along the z direction. The
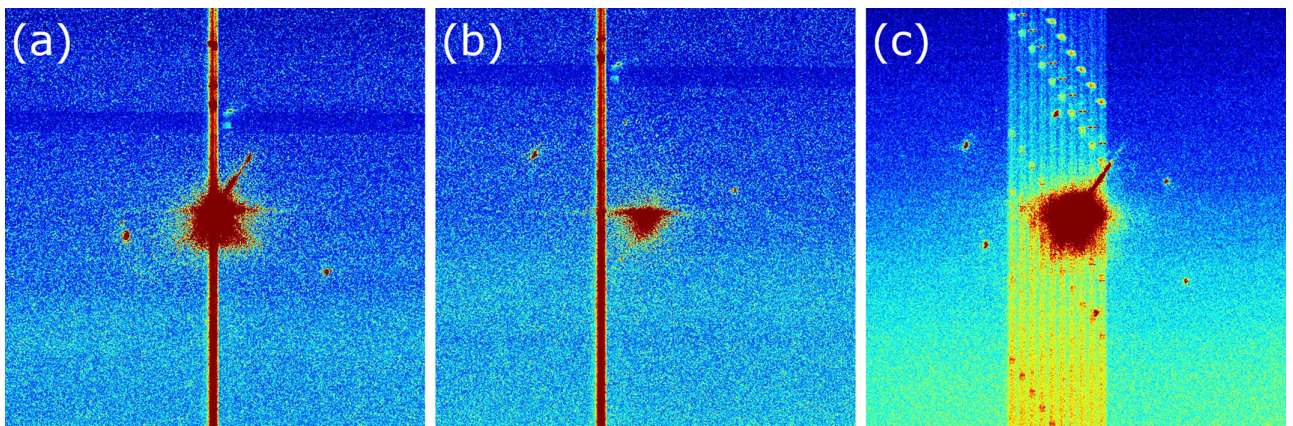

FIG. 4. Images of the surface-pinned skyrmion state at 5 eV below the Cu L_3 edge; (a) and (b) show different images captured on an area detector at different diffractometer $|q|$ values. Off the resonance energy, the x-ray penetration depth significantly increases, making features in reciprocal space more pointlike and requiring that $|q|$ be scanned to image all six magnetic satellites. Due to decreased intensity, a line of damaged pixels is visible, but should be ignored. (c) The summation of the ten images taken at different $|q|$ values from which (a) and (b) were taken. The line of damaged pixels seen in (a) and (b) is blurred across this subfigure, but is an artifact of the image alignment process and should be ignored.
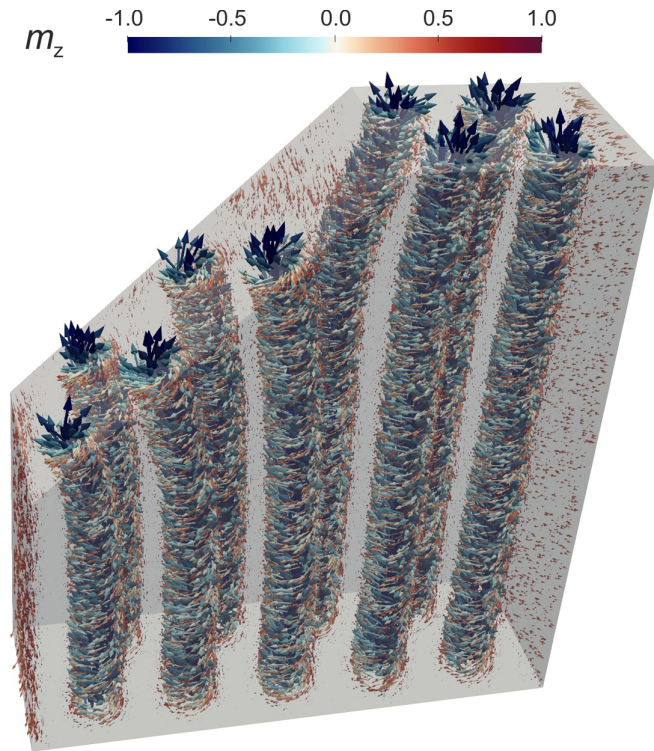
FIG. 5. A micromagnetic simulation of skyrmion strings near a tilted surface. Approximately one in four finite difference cells were randomly selected to be rendered, with the cell's magnetization represented by an arrow whose length is scaled by the magnetization's z component (with $m_z = 1$ having length 0 and $m_z = -1$ having maximal length).

simulation was then relaxed using the `Fidimag` package [30]. The ground state obtained as a result of this energetic relaxation is displayed in Fig. 5, which shows the minimum energy configuration for skyrmions incident on a tilted surface is reached when the skyrmions cant towards the surface.

The physical origin of this effect is related to energy densities. In materials with a free energy described by Eq. (3), the magnetic moments at the surface of the material always become twisted [19]. These so-called surface twist instabilities are nothing but kink solutions to the sine-Gordon equation, which one also encounters when studying the chiral soliton lattice state [31–33].

This surface-twist state has an extremely low energy density. The complicated skyrmion structures shown in Fig. 5 can be simply explained by the simulation attempting to maximize the area of surface-twist instabilities at the surface of the material. So, skyrmions are energetically obliged to become hexagonally close packed at the surface, even though the skyrmions in this simulation are not conically modulated (and have repulsive interskyrmion interactions).

Summary. An experiment has been carried out, carefully overcoming magnetic truncation rod effects, to show that skyrmions become pinned to surfaces. This data has been backed up by numerical calculations which show exactly the same effect, that near the surface of materials skyrmions stop propagating along magnetic field lines and instead prefer to align themselves with the surface normal. This curious

three-dimensional effect has a simple energetic explanation: The magnetic system wants to maximize the area on its surface that is not covered by skyrmions, so that as much as possible of the surface can be covered by the surface-twist state, which has a low energy density.

V. DISCUSSION

Due to the nanoscale size of skyrmions, it is experimentally not realistic to uniquely ascertain their three-dimensional structure (as this would generally require the unambiguous determination of a vector field with nanometer resolution throughout space). As such, the experimental state of the art does not attempt to uniquely determine the magnetization field. Instead, experimentalists acquire clues using different techniques and rely on theoretical work to put the pieces of the puzzle together. The primary purpose of the second and third sections of this work is to provide additional theoretical tools and stronger arguments that can be used to extract physical information from experimental data.

The relations derived in Sec. II can be used to check the symmetry of the *Ansätze* for the magnetization, and provide mathematical justification for the necessity of the study of three-dimensional skyrmion structures. The free energy used in Eq. (3) is minimal, but the technique used to derive these relations generalizes straightforwardly to higher order energy terms.

The conically modulated skyrmion state discussed in Sec. III has been widely investigated [10–17]. The purpose of the arguments presented in Sec. III is to provide strong mathematical justification for the observation that the coexistence of the skyrmion lattice phase and the conical phase implies that skyrmions will become conically modulated. While the nanoscale measurement of the internal structure of skyrmions is difficult, it is a relatively straightforward experimental task to measure the phase coexistence of the conical and the skyrmion lattice states.

It is worth emphasizing that we expect this conical modulation to propagate throughout skyrmion lattices—we do not expect this modulation to exist solely at the spatial boundary between the skyrmion lattice and the cone phase. In Sec. III we show that, if a skyrmion is embedded in a periodic state, the skyrmion must inherit this periodicity. Since a conically modulated skyrmion has the same periodicity as the cone phase, any skyrmion in contact with a conically modulated skyrmion should also become conically modulated. In this way, even skyrmions that are not in direct contact with the conical phase should become conically modulated, so long as the cone phase borders the skyrmion lattice *somewhere* in the material.

Additionally, many aspects of the structure of skyrmion strings (often referred to as skyrmion tubes) as they propagate through materials have been the subject of academic scrutiny. The emergent magnetic monopole dynamics at the extremity of skyrmion strings has been studied theoretically [34,35]. Skyrmion strings displaying terminations that would lead to monopolelike behavior have been recently observed directly using x-ray and electron microscopy [36–39]. Here, in Sec. IV, we study the properties of skyrmion strings that have no monopolelike properties and that terminate at the

boundaries of their confining materials. We show experimentally using REXS, and theoretically using computational micromagnetics, that this effect can be considered to be the consequence of the low energy density of the so-called surface twist instabilities present in B20 magnets [19]. The bending of skyrmion strings towards surfaces has been measured before; previously this bending has been associated with the demagnetizing field [40,41]. Our micromagnetic calculations show that this bending is very significant in the absence of the demagnetizing field. It is likely a combination of the two effects that lead to the experimental fact that skyrmion strings bend towards surfaces, but our results are particularly significant for small samples and thin films in which the demagnetizing field is smaller in magnitude.

VI. CONCLUSIONS

In conclusion, the general three-dimensional symmetry of the free energy of the magnetization has been investigated. The simple model used in this study considers only the exchange, Dzyaloshinskii-Moriya, and Zeeman interactions, but the approach can be straightforwardly extended to other energy terms. Equations that constrain the conditions for the rotational and translational symmetry of arbitrary magnetization fields have been generated independently for each term in the free energy. These conditions have been given meaningful physical interpretations. This work shows that the symmetries of the magnetization field are fundamentally three dimensional, and that one should expect magnetization structures measured in real materials to have three-dimensional properties.

The three-dimensional structure of skyrmions embedded in the conical phase was then studied. It was found that if the mathematical description of skyrmions is analytic, then skyrmions must acquire a three-dimensional modulation with the same period of the conical phase when embedded within it. This mathematical argument was then compared with numerical results, which also show that skyrmions acquire a rich periodic structure when coexisting with the conical state. The attractive nature of the interactions between conically modulated skyrmions was discussed, with reference to the fact that the dynamics of attractive skyrmions cannot be modeled using Thiele's equation.

Finally, the structure of skyrmions near a surface whose normal vector is not parallel to the direction of the applied magnetic field was studied. A REXS experiment was carried out, where it was found that skyrmion strings cant towards tilted surfaces. This result was reproduced using computational micromagnetics. The physical origin of this "surface pinning" was found to be related to the very low energy density of surface-twist instabilities. By leaning towards surfaces, skyrmions decrease the surface area that they occupy and increase the surface area that can be populated by surface-twist instabilities.

[1] S. Seki, M. Garst, J. Waizner, R. Takagi, N. D. Khanh, Y. Okamura, K. Kondou, F. Kagawa, Y. Otani, and Y. Tokura, Propagation dynamics of spin excitations along skyrmion strings, Nat. Commun. **11**, 256 (2020).

[2] N. Nagaosa and Y. Tokura, Topological properties and dynamics of magnetic skyrmions, Nat. Nanotechnol. **8**, 899 (2013).

[3] J. Zang, V. Cros, and A. Hoffmann, *Topology in Magnetism* (Springer, New York, 2018), Vol. 192.

[4] D. Cortés-Ortuño, W. Wang, M. Beg, R. A. Pepper, M.-A. Bisotti, R. Carey, M. Vousden, T. Kluyver, O. Hovorka, and H. Fangohr, Thermal stability and topological protection of skyrmions in nanotracks, Sci. Rep. **7**, 1 (2017).

[5] S.-Z. Lin, C. Reichhardt, C. D. Batista, and A. Saxena, Particle model for skyrmions in metallic chiral magnets: Dynamics, pinning, and creep, Phys. Rev. B **87**, 214419 (2013).

[6] N. S. Kiselev, A. N. Bogdanov, R. Schäfer, and U. K. Rößler, Chiral skyrmions in thin magnetic films: new objects for magnetic storage technologies?, J. Phys. D: Appl. Phys. **44**, 392001 (2011).

[7] N. Nagaosa, X. Z. Yu, and Y. Tokura, Gauge fields in real and momentum spaces in magnets: Monopoles and skyrmions, Philos. Trans. R. Soc. A **370**, 5806 (2012).

[8] A. O. Leonov, T. L. Monchesky, J. C. Loudon, and A. N. Bogdanov, Three-dimensional chiral skyrmions with attractive interparticle interactions, J. Phys.: Condens. Matter. **28**, 35LT01 (2016).

[9] J. C. Loudon, A. O. Leonov, A. N. Bogdanov, M. C. Hatnean, and G. Balakrishnan, Direct observation of attractive skyrmions and skyrmion clusters in the cubic helimagnet Cu_2OSeO_3, Phys. Rev. B **97**, 134403 (2018).

[10] H. Du, X. Zhao, F. N. Rybakov, A. B. Borisov, S. Wang, J. Tang, C. Jin, C. Wang, W. Wei, N. S. Kiselev, Y. Zhang, R. Che, S. Blügel, and M. Tian, Interaction of Individual Skyrmions in a Nanostructured Cubic Chiral Magnet, Phys. Rev. Lett. **120**, 197203 (2018).

[11] A. O. Leonov, J. C. Loudon, and A. N. Bogdanov, Spintronics via non-axisymmetric chiral skyrmions, Appl. Phys. Lett. **109**, 172404 (2016).

[12] A. O. Leonov and C. Pappas, Skyrmion clusters and conical droplets in bulk helimagnets with cubic anisotropy, Phys. Rev. B **99**, 144410 (2019).

[13] H. R. O. Sohn, S. M. Vlasov, V. M. Uzdin, A. O. Leonov, and I. I. Smalyukh, Real-space observation of skyrmion clusters with mutually orthogonal skyrmion tubes, Phys. Rev. B **100**, 104401 (2019).

[14] T.-H. Kim, H. Zhao, B. Xu, B. A. Jensen, A. H. King, M. J. Kramer, C. Nan, L. Ke, and L. Zhou, Mechanisms of skyrmion and skyrmion crystal formation from the conical phase, Nano Lett. **20**, 4731 (2020).

[15] A. O. Leonov, C. Pappas, and I. I. Smalyukh, Field-driven metamorphoses of isolated skyrmions within the conical state of cubic helimagnets, Phys. Rev. B **104**, 064432 (2021).

[16] A. O. Leonov, Surface anchoring as a control parameter for shaping skyrmion or toron properties in thin layers of chiral nematic liquid crystals and noncentrosymmetric magnets, Phys. Rev. E **104**, 044701 (2021).

[17] A. O. Leonov, Skyrmion clusters and chains in bulk and thin-layered cubic helimagnets, Phys. Rev. B **105**, 094404 (2022).

[18] U. K. Rößler, A. A. Leonov, and A. N. Bogdanov, Chiral skyrmionic matter in non-centrosymmetric magnets, J. Phys.: Conf. Ser. **303**, 012105 (2011).

[19] S. A. Meynell, M. N. Wilson, H. Fritzsche, A. N. Bogdanov, and T. L. Monchesky, Surface twist instabilities and skyrmion states in chiral ferromagnets, Phys. Rev. B **90**, 014406 (2014).

[20] R. Brearton, G. van der Laan, and T. Hesjedal, Magnetic skyrmion interactions in the micromagnetic framework, Phys. Rev. B **101**, 134422 (2020).

[21] D. M. Burn, R. Brearton, K. J. Ran, S. L. Zhang, G. van der Laan, and T. Hesjedal, Periodically modulated skyrmion strings in Cu_2OSeO_3, npj Quant. Mater. **6**, 73 (2021).

[22] A. A. Thiele, Steady-State Motion of Magnetic Domains, Phys. Rev. Lett. **30**, 230 (1973).

[23] D. Capic, D. A. Garanin, and E. M. Chudnovsky, Skyrmion–skyrmion interaction in a magnetic film, J. Phys.: Condens. Matter **32**, 415803 (2020).

[24] S. L. Zhang, A. Bauer, H. Berger, C. Pfleiderer, G. van der Laan, and T. Hesjedal, Resonant elastic x-ray scattering from the skyrmion lattice in Cu_2OSeO_3, Phys. Rev. B **93**, 214420 (2016).

[25] S. L. Zhang, A. Bauer, D. M. Burn, P. Milde, E. Neuber, L. M. Eng, H. Berger, C. Pfleiderer, G. van der Laan, and T. Hesjedal, Multidomain skyrmion lattice state in Cu_2OSeO_3, Nano Lett. **16**, 3285 (2016).

[26] I. K. Robinson, Crystal truncation rods and surface roughness, Phys. Rev. B **33**, 3830 (1986).

[27] G.M. Watson, D. Gibbs, G.H. Lander, B.D. Gaulin, L.E. Berman, H. Matzke, and W. Ellis, X-Ray Scattering Study of the Magnetic Structure near the (001) Surface of UO_2, Phys. Rev. Lett. **77**, 751 (1996).

[28] K. Ran, Y. Liu, Y. Guang, D. M. Burn, G. van der Laan, T. Hesjedal, H. Du, G. Yu, and S. Zhang, Creation of a Chiral Bobber Lattice in Helimagnet-Multilayer Heterostructures, Phys. Rev. Lett. **126**, 017204 (2021).

[29] S. Zhang, G. van der Laan, J. Müller, L. Heinen, M. Garst, A. Bauer, H. Berger, C. Pfleiderer, and T. Hesjedal, Reciprocal space tomography of 3D skyrmion lattice order in a chiral magnet, Proc. Natl. Acad. Sci. USA **115**, 6386 (2018).

[30] M.-A. Bisotti, D. Cortés-Ortuño, R. A. Pepper, W. Wang, M. Beg, T. Kluyver, and H. Fangohr, Fidimag—a finite difference atomistic and micromagnetic simulation package, J. Open Res. Softw. **6**, 22 (2018).

[31] J. Rubinstein, Sine-Gordon equation, J. Math. Phys. **11**, 258 (1970).

[32] J.-I. Kishine, K. Inoue, and Y. Yoshida, Synthesis, structure and magnetic properties of chiral molecule-based magnets, Prog. Theor. Phys. Suppl. **159**, 82 (2005).

[33] Y. Togawa, T. Koyama, K. Takayanagi, S. Mori, Y. Kousaka, J. Akimitsu, S. Nishihara, K. Inoue, A. S. Ovchinnikov, and J. Kishine, Chiral Magnetic Soliton Lattice on a Chiral Helimagnet, Phys. Rev. Lett. **108**, 107202 (2012).

[34] P. Milde, D. Köhler, J. Seidel, L. M. Eng, A. Bauer, A. Chacon, J. Kindervater, S. Mühlbauer, C. Pfleiderer, S. Buhrandt, C. Schütte, and A. Rosch, Unwinding of a skyrmion lattice by magnetic monopoles, Science **340**, 1076 (2013).

[35] F. Kagawa, H. Oike, W. Koshibae, A. Kikkawa, Y. Okamura, Y. Taguchi, N. Nagaosa, and Y. Tokura, Current-induced viscoelastic topological unwinding of metastable skyrmion strings, Nat. Commun. **8**, 1332 (2017).

[36] M. T. Birch, D. Cortes-Ortuno, L. A. Turnbull, M. N. Wilson, F. Groß, N. Träger, A. Laurenson, N. Bukin, S. H. Moody, M. Weigand, G. Schütz, H. Popescu, R. Fan, P. Steadman, J. A. T. Verezhak, G. Balakrishnan, J. C. Loudon, A. C. Twitchett-Harrison, O. Hovorka, H. Fangohr *et al.*, Real-space imaging of confined magnetic skyrmion tubes, Nat. Commun. **11**, 1726 (2020).

[37] M. T. Birch, D. Cortes-Ortuno, K. Litzius, S. Wintz, F. Schulz, M. Weigand, A. Stefancic, D. A. Mayoh, G. Balakrishnan, P. D. Hatton, and G. Schütz, Toggle-like current-induced Bloch point dynamics of 3D skyrmion strings in a room temperature nanowire, Nat. Commun. **13**, 3630 (2022).

[38] X. Yu, J. Masell, F. S. Yasin, K. Karube, N. Kanazawa, K. Nakajima, T. Nagai, K. Kimoto, W. Koshibae, Y. Taguchi, N. Nagaosa, and Y. Tokura, Real-space observation of topological defects in extended skyrmion-strings, Nano Lett. **20**, 7313 (2020).

[39] N. Mathur, F. S. Yasin, M. J. Stolt, T. Nagai, K. Kimoto, H. Du, M. Tian, Y. Tokura, X. Yu, and S. Jin, In-plane magnetic field-driven creation and annihilation of magnetic skyrmion strings in nanostructures, Adv. Funct. Mater. **31**, 2008521 (2021).

[40] M. Crisanti, M. T. Birch, M. N. Wilson, S. H. Moody, A. Štefančič, B. M. Huddart, S. Cabeza, G. Balakrishnan, P. D. Hatton, and R. Cubitt, Position-dependent stability and lifetime of the skyrmion state in nickel-substituted Cu_2OSeO_3, Phys. Rev. B **102**, 224407 (2020).

[41] T. Reimann, A. Bauer, C. Pfleiderer, P. Böni, P. Trtik, A. Tremsin, M. Schulz, and S. Mühlbauer, Neutron diffractive imaging of the skyrmion lattice nucleation in MnSi, Phys. Rev. B **97**, 020406(R) (2018).